

Multilayered noise model for transport in complex environmentsNikolaos K. Voulgarakis *Department of Mathematics and Statistics, Washington State University, Pullman, Washington 99164, USA*

(Received 18 July 2023; accepted 9 November 2023; published 4 December 2023; corrected 28 February 2024 and 12 March 2024)

Transport in complex fluidic environments often exhibits transient subdiffusive dynamics accompanied by non-Gaussian probability density profiles featuring a nonmonotonic non-Gaussian parameter. Such properties cannot be adequately explained by the original theory of Brownian motion. Based on an extension of kinetic theory, this study introduces a chain of hierarchically coupled random walks approach that effectively captures all these intriguing characteristics. If the environment consists of a series of independent white noise sources, then the problem can be expressed as a system of hierarchically coupled Ornstein-Uhlenbeck equations. Due to the linearity of the system, the most essential transport properties have a closed analytical form.

DOI: [10.1103/PhysRevE.108.064105](https://doi.org/10.1103/PhysRevE.108.064105)**I. INTRODUCTION**

Brownian motion (BM), originally explored through systematic experiments by Brown [1], and later examined theoretically by Einstein [2] and Smoluchowski [3], is an exceptionally ubiquitous phenomenon with applications spanning across a wide range of disciplines. Mathematically, the probability density function (PDF) of a Brownian particle's position is modeled by the diffusion equation. This formulation gives rise to two characteristic features of BM: the position follows a normal distribution, and the mean square displacement (MSD) equals $2Dt$, where D represents the diffusivity of the Brownian particle and t denotes time. Langevin [4] and later Ornstein and Uhlenbeck (OU) [5] demonstrated that a Brownian particle displays a ballistic behavior prior to reaching the terminal diffusive regime.

Recent experimental and molecular dynamics (MD) studies have revealed significant deviations from the predictions of BM theory. Such deviations have been observed in soft biological systems [6–11], supercooled and ionic liquids [12–17], granular and glassy materials [18–26], in confined spaces and near interfaces [27,28], as well as diffusion under the influence of optical speckle fields [29]. In the seminal work [6], it was demonstrated that particles can exhibit Fickian diffusion with non-Gaussian characteristics for the entire duration of the experimental observation. In particular, it was shown that the PDF of the particle's position is Laplacian with average length $l(t) \propto \sqrt{t}$. In other cases, MSD profiles may exhibit three distinct time regimes (see, for example, Refs. [13,29]). Initially, a short-term behavior characterized by ballistic or diffusive motion is observed, followed by a subdiffusive regime, which eventually transitions to a terminal diffusive motion with a smaller diffusion coefficient. Notably, even during the terminal diffusive behavior, the particle's position remains non-Gaussian for a significant period before returning to a Gaussian distribution. These phenomena have given rise to a new term known as Fickian yet non-Gaussian

diffusion (FnGD). In short, a particle undergoing FnGD may exhibit some or all of the following key properties: (a) Fickian diffusion or transient subdiffusion, (b) non-Gaussian PDF, and (c) nonmonotonic non-Gaussian parameter (NGP).

From a theoretical perspective, anomalous diffusion has been successfully modeled in various studies involving continuous-time random walks (CTRW) [30–34], fractional Fokker-Planck equations [35,36], and fractional BM [37] (refer to Ref. [38] for a review on anomalous diffusion). However, these approaches have limitations in explaining Fickian MSD profiles with transient non-Gaussian characteristics. Superstatistics, initially presented by Beck and Cohen [39], assumes that complex environments introduce random variations in the diffusivity of the particles (see Ref. [40] for a review). By considering a given probability density for the diffusivity, this approach can describe Fickian MSD with non-Gaussian characteristics. However, it does not fully address the transient MSD and the transition to Gaussian process at longer times. In another seminal work [41], Chubynsky and Slater introduced the concept of diffusive (stochastic) diffusivity, which was subsequently rigorously analyzed in Refs. [42,43]. This approach treats diffusivity as a stochastic process described by a mean reverting method, such as the OU or Cox-Ingersoll-Ross (CIR) equation. The finite correlation time associated with diffusivity allows for the description of a non-Gaussian PDF that eventually converges to a Gaussian distribution over longer timescales. However, this method cannot describe the transient subdiffusion and the nonmonotonic NGP. In a recent study, Song *et al.* developed a random walk model that exhibits transient subdiffusion accompanied by a nonmonotonic NGP [16]. The non-Gaussian PDF was addressed by utilizing a mixture of stochastic diffusivity models. Mora and Pomeau have successfully implemented a two-state model to show that diffusion in a dilute field of traps is Fickian with transient non-Gaussian characteristics [44]. The transient anomalous diffusion was not discussed in their work.

This article proposes that particles moving in complex environments are *hierarchically* influenced by a series of independent noise sources, each operating at a different timescale. This approach can be considered as a hierarchical

*Corresponding author: n.voulgarakis@wsu.edu

implementation of kinetic theory and can be mathematically formulated as a chain of hierarchically coupled random walks. Specifically, when considering white noise sources, the problem reduces to a system of stochastic differential equations (SDEs) with an analytical solution. The resulting MSD profile captures a diverse range of behaviors observed in various experiments and MD simulations of systems with dynamic or structural heterogeneity. Furthermore, if the noise sources represent BMs with stochastic diffusivity, then this approach enables an effective description of all three major features of FnGD: a Fickian or transient subdiffusive MSD, a transient non-Gaussian PDF, and a nonmonotonic NGP.

This paper is organized as follows. Section II introduces the multilayered noise model and presents the associated system of OU equations. Section III focuses exclusively on analyzing the case where only two noise levels are involved. In particular, Sec. III A presents the analytical solutions and Sec. III B discusses the existence of a nonequilibrium steady state distribution (NESS). Sections III C and III D are devoted to the mean squared displacement (MSD) and the different behaviors it exhibits. Section III E presents three aspects of FnGD that this model captures by applying the stochastic diffusivity concept. The paper concludes with a summary and discussion in Sec. IV.

II. MULTILAYERED NOISE MODEL

Assume a particle (tracer) moving in a one-dimensional complex environment comprising of n independent sources of noise, $B_t^{(i)}$, where $i = 1, \dots, n$. Let us denote the position and velocity of the particle as $X_t^{(n)}$ and $V_t^{(n)}$, respectively. This study suggests that the velocity can be modeled by the following equation:

$$V_t^{(n)} = \frac{dX_t^{(n)}}{dt} = \sum_{i=1}^n \gamma_i (B_t^{(i)} - X_t^{(i)}), \quad (1)$$

where each γ_i represents a positive constant. Any state $(X_t^{(i)}, V_t^{(i)})$ with $i < n$ is governed by the same equation and represents the tracer's position and velocity, assuming only the first $1, 2, \dots, i$ noise sources are in effect. The observable state in an experimental measurement is $(X_t^{(n)}, V_t^{(n)})$. Note that $X_t^{(j)}$ affects $X_t^{(i)}$ only if $j < i$. Therefore, Eq. (1) is a series of hierarchically coupled random walks. In general, $B_t^{(i)}$ can be any realistic stochastic process. For the sake of simplicity, it is assumed that each $B_t^{(i)}$ describes a BM with diffusivity D_i , meaning $dB_t^{(i)} = \sigma_i dW_t^{(i)}$, where $\sigma_i = \sqrt{2D_i}$, and $W_t^{(i)}$ are independent Wiener processes. If we define the difference

$$u_t^{(i)} = B_t^{(i)} - X_t^{(i)}, \quad (2)$$

and note that

$$V_t^{(i)} = \sum_{j=1}^i \gamma_j u_t^{(j)}, \quad (3)$$

then Eq. (1) can be alternatively written as

$$dV_t^{(n)} = -\gamma_n u_t^{(n)} dt + \sigma_n dW_t^{(n)} - \sum_{i=1}^{n-1} \gamma_i u_t^{(i)} dt, \quad (4)$$

or

$$dV_t^{(n)} = -\gamma_n V_t^{(n)} dt + \gamma_n \sigma_n dW_t^{(n)} + dV_t^{(n-1)}. \quad (5)$$

Equations (4) and (5) describe a system of n hierarchically coupled OU processes. Under these assumptions, Eqs. (1), (4), and (5) represent systems of linear SDEs in the narrow sense with a strong analytical solution [45]. All solutions $\mathbf{X}_t = (X_t^{(1)}, \dots, X_t^{(n)})^T$, $\mathbf{u}_t = (u_t^{(1)}, \dots, u_t^{(n)})^T$, and $\mathbf{V}_t = (V_t^{(1)}, \dots, V_t^{(n)})^T$ are n -variate Gaussian processes [45]. Note that for $n = 1$, Eqs. (4) and (5) are standard OU equations.

Equation (1) is based on the concept of kinetic theory, according to which the motion of a particle is a combination of alternating ballistic drifts and random collisions with the surrounding fluid molecules. Mathematically, the collision points belong to a random path following Brownian motion [46]. This physical mechanism leads to a ballistic motion at short times and pure Brownian at long timescales. One way to describe such stochastic paths is the Langevin equation, which models the particle's velocity as an exponentially correlated stochastic process (OU). Here, it is shown that Eq. (1) for $n = 1$ provides an alternative approach to capture the ballistic-to-diffusive crossover. Figure 1(a) illustrates the solution of Eq. (1) for $D_1 = 1$ and $\gamma_1 = 100$. Initially, the particle drifts toward $B_t^{(1)}$, and when their paths intersect, the particle starts moving in the opposite direction until their paths cross again. These path crossings occur in the vicinity of $B_t^{(1)}$, which means they can be seen as collisions with the surrounding molecules. In Fig. 1(a), we observe that despite the random collisions, the particle's motion is predominantly ballistic in the short term. However, as depicted in Fig. 1(b), the motion eventually resembles the standard Brownian process, indicating a transition from ballistic to diffusive dynamics. This transition is shown in Fig. 1(c), where the MSD versus time is demonstrated. In simpler physical terms, Eq. (1) with $n = 1$ represents a particle that is confined near $B_t^{(1)}$ by a linear force field. If we consider further collisions with molecules of another fluid, then the same physical interpretation can be used to add a second random drift. This approach will yield Eq. (1) with $n = 2$. If $D_2 < D_1$, then the second noise source introduces a caging effect in the system. This trapping leads to a transient subdiffusion before the tracer eventually adapts the diffusive behavior of $B_t^{(2)}$. Considering the hierarchical influence of n noise sources leads to Eq. (1). This approach with $n = 2$ can describe a wide range of experimental and MD observations, as demonstrated below.

III. SPECIAL CASE $n = 2$

For the sake of simplicity, this work focuses only on $n = 2$. The generalization for any n is straightforward and will be presented elsewhere. To study this special case, we can either solve Eq. (1) to determine \mathbf{X}_t and subsequently differentiate to obtain \mathbf{V}_t , or alternatively, solve Eq. (5) for \mathbf{V}_t and then integrate to compute \mathbf{X}_t . However, given the linear dependence of both \mathbf{X}_t and \mathbf{V}_t on \mathbf{u}_t [see Eqs. (2) and (3)], it is more convenient to address Eq. (4).

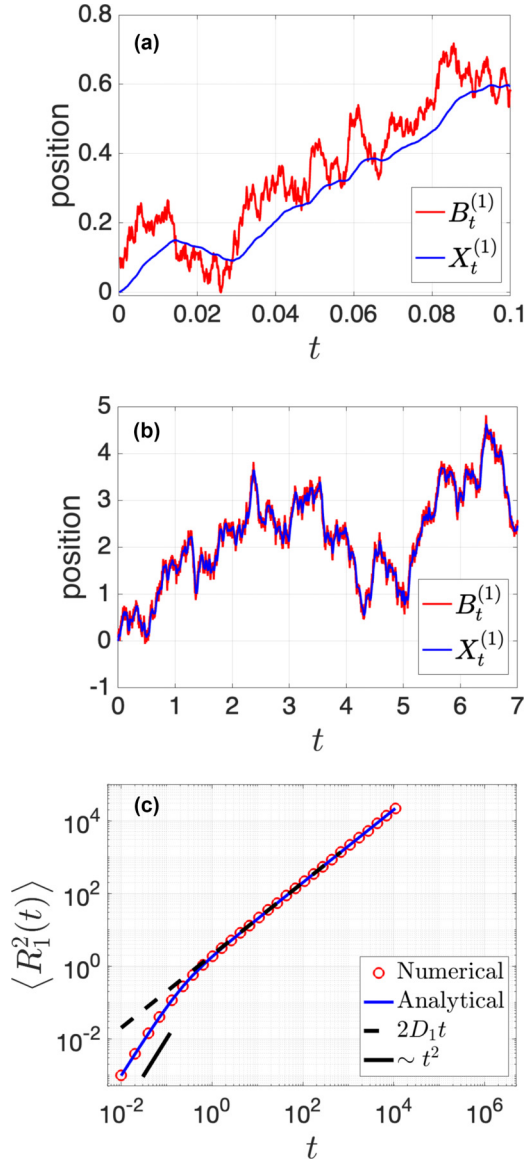


FIG. 1. Stochastic paths of $B_t^{(1)}$ (red line) and $X_t^{(1)}$ (blue line) for (a) short-term and (b) long-term periods. Here, $B_t^{(1)}$ represents a Brownian motion with diffusivity $D_1 = 1$. Panel (c) depicts the MSD vs time profile. MSD is defined as $\langle R_1^2(t) \rangle$, where $R_1(t) = X_t^{(1)} - X_0^{(1)}$ is the displacement from the initial condition, and $\langle \cdot \rangle$ represents ensemble average. The solid blue line and red circles represent the analytical and numerical solutions, respectively. The dashed line indicates linear MSD with $D_1 = 1$, and the solid line represents ballistic MSD, i.e., $\text{MSD} \sim t^2$. Appendix A 4 provides details about the numerical methods and statistical average.

A. Analytical solution

For $n = 2$, Eq. (4) reads

$$\begin{aligned} du_t^{(1)} &= -\gamma_1 u_t^{(1)} dt + \sigma_1 dW_t^{(1)}, \\ du_t^{(2)} &= -\gamma_1 u_t^{(1)} dt - \gamma_2 u_t^{(2)} dt + \sigma_2 dW_t^{(2)}. \end{aligned} \quad (6)$$

In standard vector-matrix notation, Eq. (6) can be expressed as

$$d\mathbf{u}_t = -\mathbf{\Gamma}\mathbf{u}_t dt + \mathbf{\Sigma}d\mathbf{W}_t, \quad (7)$$

where $\mathbf{u}_t = (u_t^{(1)}, u_t^{(2)})^T$, $\mathbf{W}_t = (W_t^{(1)}, W_t^{(2)})^T$. Here,

$$\mathbf{\Gamma} = \begin{pmatrix} \gamma_1 & 0 \\ \gamma_1 & \gamma_2 \end{pmatrix} \quad \text{and} \quad \mathbf{\Sigma} = \begin{pmatrix} \sigma_1 & 0 \\ 0 & \sigma_2 \end{pmatrix}$$

represent the dissipation and stochastic matrix, respectively. Furthermore, $\mathbf{\Sigma}\mathbf{\Sigma}^T = 2\mathbf{D}$, where \mathbf{D} is diagonal and defines the diffusivity matrix. The solution to Eq. (7) is given by

$$\mathbf{u}_t = \mathbf{G}(t)\mathbf{u}_0 + \int_0^t \mathbf{G}(t-s)\mathbf{\Sigma}d\mathbf{W}_s, \quad (8)$$

where $\mathbf{G}(t) = \exp(-\mathbf{\Gamma}t)$ [45]. By employing this solution, we can determine \mathbf{X}_t and \mathbf{V}_t through Eqs. (2) and (3), respectively.

Let us denote the mean vector and two-time correlation matrix as $\mathbf{M}(t) = \langle \mathbf{u}_t \rangle$ and $\mathbf{C}(t, s) = \langle \mathbf{u}_t \mathbf{u}_s^T \rangle$, respectively. By utilizing the zero-mean and isometry properties of Itô integrals, we obtain the mean:

$$\mathbf{M}(t) = \mathbf{G}(t)\mathbf{u}_0, \quad (9)$$

and the same-time autocorrelation matrix

$$\mathbf{C}(t, t) = \mathbf{G}(t)\mathbf{C}(0, 0)\mathbf{G}^T(t) + 2 \int_0^t \mathbf{G}(t-s)\mathbf{D}\mathbf{G}^T(t-s)ds, \quad (10)$$

The covariance matrix is given by

$$\mathbf{K}(t) = \mathbf{C}(t, t) - \mathbf{G}(t)\mathbf{C}(0, 0)\mathbf{G}^T(t). \quad (11)$$

The remainder of this section explores the fundamental properties of this solution.

B. Nonequilibrium steady state

In the long-term limit ($t \rightarrow \infty$), the mean vanishes,

$$\mathbf{M}_\infty = 0, \quad (12)$$

and the covariance becomes constant,

$$\mathbf{K}_\infty = \begin{pmatrix} \frac{\sigma_1^2}{2\gamma_1} & -\phi_0 \frac{\sigma_1^2}{2\gamma_1} \\ -\phi_0 \frac{\sigma_1^2}{2\gamma_1} & \frac{\sigma_2^2}{2\gamma_2} + \phi_0 \frac{\sigma_1^2}{2\gamma_2} \end{pmatrix}, \quad (13)$$

where $\phi_0 = \frac{\gamma_1}{\gamma_1 + \gamma_2}$. Consequently, the system has a stationary distribution given by

$$P(\mathbf{u}_t) = \frac{1}{\sqrt{2\pi}|\mathbf{K}_\infty|^{1/2}} \exp\left(-\frac{1}{2}\mathbf{u}_t^T \mathbf{K}_\infty^{-1} \mathbf{u}_t\right). \quad (14)$$

However, since $\mathbf{\Gamma}\mathbf{D} \neq \mathbf{D}\mathbf{\Gamma}^T$, the system (7) is time irreversible and Eq. (14) describes a NESS [47,48].

Using Eqs. (3), (12), and (13), it is easy to show that the tracer's velocity ($V_t^{(2)}$) exhibits a normal steady-state distribution with zero mean and variance $\beta_\infty = \phi_0 \frac{\gamma_1 \sigma_1^2}{2} + \frac{\gamma_2 \sigma_2^2}{2}$. Furthermore, the two-times velocity autocorrelation function (ACF) is

$$\langle V_t^{(2)} V_s^{(2)} \rangle = \phi_1 \frac{\gamma_1 \sigma_1^2}{2} e^{-\gamma_1 |t-s|} + \phi_2 \frac{\gamma_2 \sigma_2^2}{2} e^{-\gamma_2 |t-s|}, \quad (15)$$

where $\langle \cdot \rangle$ indicates the ensemble average, $\phi_1 = \gamma_1^2 / (\gamma_1^2 - \gamma_2^2)$ and $\phi_2 = 1 - \phi_1 (\sigma_1 / \sigma_2)^2$. Depending on the parameters values, the relaxation of the velocity ACF can be strictly positive

or exhibit negative values. The latter indicates anticorrelation resulting from trapping events.

C. Transient subdiffusion

The tracer's MSD is defined as $\langle R_2^2(t) \rangle$, where $R_2(t) = X_t^{(2)} - X_0^{(2)}$ is the displacement from the initial condition. The analytical formula for $R_2(t)$ is given in Appendix A 1, Eq. (A4). Assuming that the initial conditions for $u_0^{(i)}$ are drawn from the stationary bivariate normal distribution of Eq. (14), the MSD of the tracer reads

$$\begin{aligned} \langle R_2^2(t) \rangle &= \sigma_2^2 t - \frac{\sigma_2^2}{\gamma_2} (1 - e^{-\gamma_2 t}) + \phi_0 \frac{\sigma_1^2}{2\gamma_2} (1 - e^{-\gamma_2 t})^2 \\ &+ \phi_1 \frac{\sigma_1^2}{\gamma_1} (1 - e^{-\gamma_2 t})(e^{-\gamma_1 t} - e^{-\gamma_2 t}) \\ &+ \bar{\gamma}^2 \frac{\sigma_1^2}{2\gamma_1} [h(t) + (e^{-\gamma_1 t} - e^{-\gamma_2 t})^2], \end{aligned} \quad (16)$$

where

$$h(t) = 2\gamma_1 \left(\frac{1 - e^{-2\gamma_1 t}}{2\gamma_1} + \frac{1 - e^{-2\gamma_2 t}}{2\gamma_2} - 2 \frac{1 - e^{-(\gamma_1 + \gamma_2)t}}{\gamma_1 + \gamma_2} \right),$$

and $\bar{\gamma} = \gamma_1 / (\gamma_1 - \gamma_2)$. Two limits are worth noting. First, in line with the qualitative analysis of Sec. II, at long times ($t \rightarrow \infty$), $\langle R_2^2(t) \rangle \rightarrow 2D_2 t$, meaning the tracer follows $B_t^{(2)}$. Second, as time approaches zero, all linear terms vanish, resulting in a ballistic motion with MSD $\langle R_2^2(t) \rangle \sim t^2$.

Figure 2 compares the analytical and numerical MSD for three different sets of parameters. In all three cases, the parameters for the first level of noise are $D_1 = 1$ and $\gamma_1 = 10$. The observed MSD profiles are a combination of ballistic, subdiffusive, and diffusive dynamics. Figure 2(a), illustrates a system where the parameters of the second level of noise are $D_2 = 0.01$ and $\gamma_2 = 0.02$. We still observe the initial ballistic to diffusive transition caused by the first level of noise [see Fig. 1(c)]; however, since $D_2 < D_1$, the tracer subsequently experiences a transient subdiffusive regime before eventually converging to the diffusive behavior associated with the second noise. The duration of the initial ballistic and diffusive regimes can be controlled by adjusting the relaxation parameters γ_1 and γ_2 . As demonstrated in Fig. 2(b), by increasing γ_2 ($= 1$), the initial diffusive regime can be eliminated. This scenario corresponds to a process characterized by a ballistic to subdiffusive to diffusive transition, which has been observed, for instance, in supercooled liquids [12,26]. If, instead, we significantly increase γ_1 ($= 10^3$), then the ballistic regime can be eliminated within the time resolution utilized in Fig. 2(c). This scenario corresponds to a diffusive to subdiffusive back to diffusive behavior, which has also been experimentally observed in speckle field experiments [29] and suspensions of charged vesicles in water [49].

D. Overdamped limit

In the limit of very large γ_1 [Fig. 2(c)], the first equation of Eq. (6) becomes $\gamma_1 u_t^{(1)} dt \approx \sigma_1 dW_t^{(1)}$. Therefore, Eq. (1) reduces to

$$dX_t^{(2)} = \gamma_2 (B_t^{(2)} - X_t^{(2)}) dt + \sigma_1 dW_t^{(1)}. \quad (17)$$

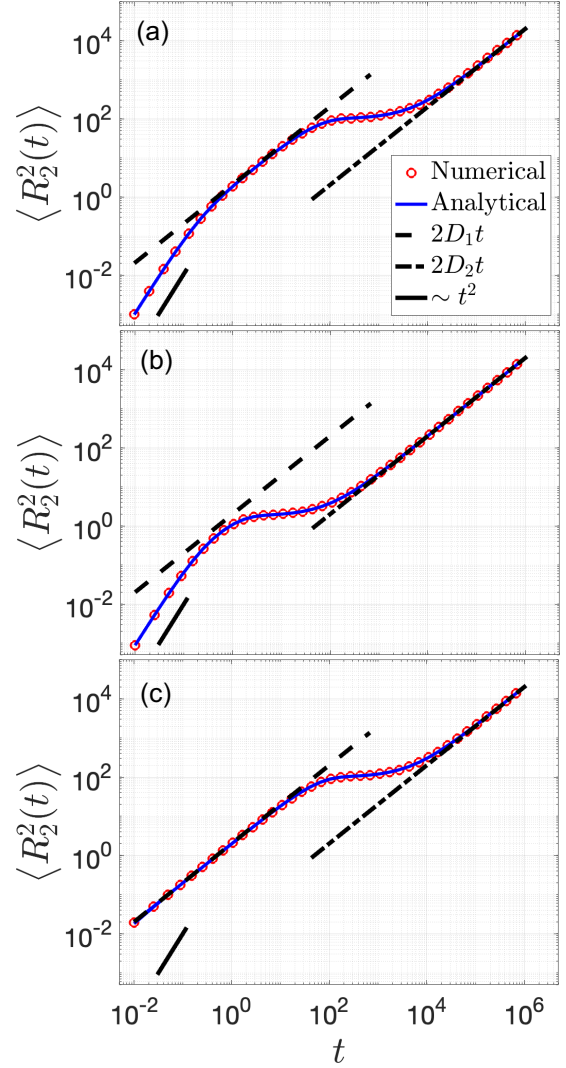


FIG. 2. MSD vs time for $n = 2$ for various system parameters. The relaxation parameters are set to (a) $\gamma_1 = 10$ and $\gamma_2 = 0.02$, (b) $\gamma_1 = 10$ and $\gamma_2 = 1$, and (c) $\gamma_1 = 10^3$ and $\gamma_2 = 0.02$. Dashed and dashed-dotted lines indicate pure diffusion MSDs with $D_1 = 1$ and $D_2 = 0.01$, respectively, while the solid black line represents the ballistic MSD, i.e., MSD $\propto t^2$. Solid blue line and red circles represent the analytical and numerical solutions, respectively. Appendix A 4 provides details about the numerical methods and statistical average.

The analytical solution to this equation is presented in Appendix A 2. Note that the second term in Eq. (17) is a pure BM, and as a result, the velocity of the particle is not defined. The analytical relation for the MSD is

$$\langle R_2^2(t) \rangle = 2D_2 t + \frac{2(D_1 - D_2)}{\gamma_2} (1 - e^{-\gamma_2 t}). \quad (18)$$

Notably, in the short term limit ($t \rightarrow 0$), $\langle R_2^2(t) \rangle \sim 2D_1 t$, while in the long-term limit ($t \rightarrow \infty$), $\langle R_2^2(t) \rangle \sim 2D_2 t$. This MSD expression is an excellent approximation of Eq. (16) in the limit of large γ_1 [see Fig. 2(c)]. Of particular interest is the case of $D_1 = D_2 = D$, where the MSD simplifies to $\langle R_2^2(t) \rangle = 2Dt$ for all $t \geq 0$, indicating *pure* Fickian behavior.

E. Fickian yet non-Gaussian diffusion

In addition to the MSD and velocity's probability density and autocorrelation functions, this work also focuses on the PDF of the tracer's displacement as a function of time $P(R_2, t)$, and the NGP defined as $\alpha_2^{(2)} = \langle R_2^4(t) \rangle / \langle R_2^2(t) \rangle^2 - 3$. Since $X_t^{(2)}$ is a Gaussian process, $\alpha_2^{(2)} = 0$.

The Gaussian profile of the solution changes if the noise $B_t^{(2)}$ is generated by a complex environment with structural or dynamic heterogeneity. Biological systems are a good example of structural heterogeneity, where the surrounding fluid is composed of particles with different masses, structures, and sizes. On the other hand, dynamic heterogeneity can be seen in materials undergoing a glass transition. In these systems, particles continuously jump between different traps formed by neighboring molecules, which gives rise to dynamic heterogeneity. In both cases, the heterogeneity in the environment, whether structural or dynamic, introduces variations in the diffusivity and affects the particle's motion. It is reasonable to assume that the diffusivity D_2 is a random variable with a specific probability distribution [39,41]. Following the work of Ref. [41], the diffusivity is modeled stochastically as $D_2(t) = D_2 y_t^2$, where y_t is an OU process with a variance of $\beta^2/2\lambda = 1$. Here, λ and β represent the dissipation and magnitude of the random fluctuations, respectively. Under these assumptions, $\langle D_2(t) \rangle = D_2$ and $\langle D_2(t)D_2(0) \rangle = D_2^2 \exp(-\lambda t)$. Studies have demonstrated that BM with stochastic diffusivity exhibits a purely diffusive MSD accompanied by a transient non-Gaussian PDF [41–43]. The observed NGP initially assumes nonzero values that gradually decrease to zero. This behavior deviates from some experimental observations, where the NGP initially starts from zero, increases to a maximum value, and subsequently decreases back to zero in the long-term limit.

By introducing $B_t^{(2)} = \int_0^t \sqrt{2D_2(s)} dW_s^{(2)}$ in Eq. (1), it is possible to construct a stochastic process that captures all three major characteristics of FnGD: a transient subdiffusive MSD, a transient non-Gaussian PDF, and a nonmonotonic NGP. The typical ballistic-to-subdiffusive-to-diffusive behavior is demonstrated in Fig. 3(a). It is important to underline that although the velocity and displacement of the particle are no longer a Gaussian process, the analytical expressions for the MSD still hold (see Appendix A 3). The validity of this remark is also demonstrated by the excellent comparison between the analytical and numerical MSD profiles [see Fig. 3(a)]. Thus, with or without stochastic diffusivity, the MSD profiles remain unchanged.

To better illustrate the non-Gaussianity in the PDF, the displacement is rescaled as $r_2 = R_2(t)/\sqrt{\langle R_2^2(t) \rangle}$, and the PDF as $p(|r_2|, t) = P(|R_2|, t)/\sqrt{\langle R_2^2(t) \rangle}$. In this description, all Gaussian distributions collapse to the standard normal $G(|r|) = \sqrt{2/\pi} \exp(-r^2/2)$ [29]. Figure 3(b) presents the rescaled PDF for four different times: $t = 0.01$, $t = 43$, $t = 171$, and $t = 6807$. Initially, at short times, the particle's displacement follows a Gaussian distribution. Over time, the distribution progressively diverges from the standard normal distribution, reaching a maximum deviation at around $t \approx 171$. It then gradually approaches the standard normal distribution again. Interestingly, the tails of the scaled PDF are exponential with a nondiffusive characteristic length, i.e., not proportional to \sqrt{t} [see Fig. 3(b)]. This characteristic has been

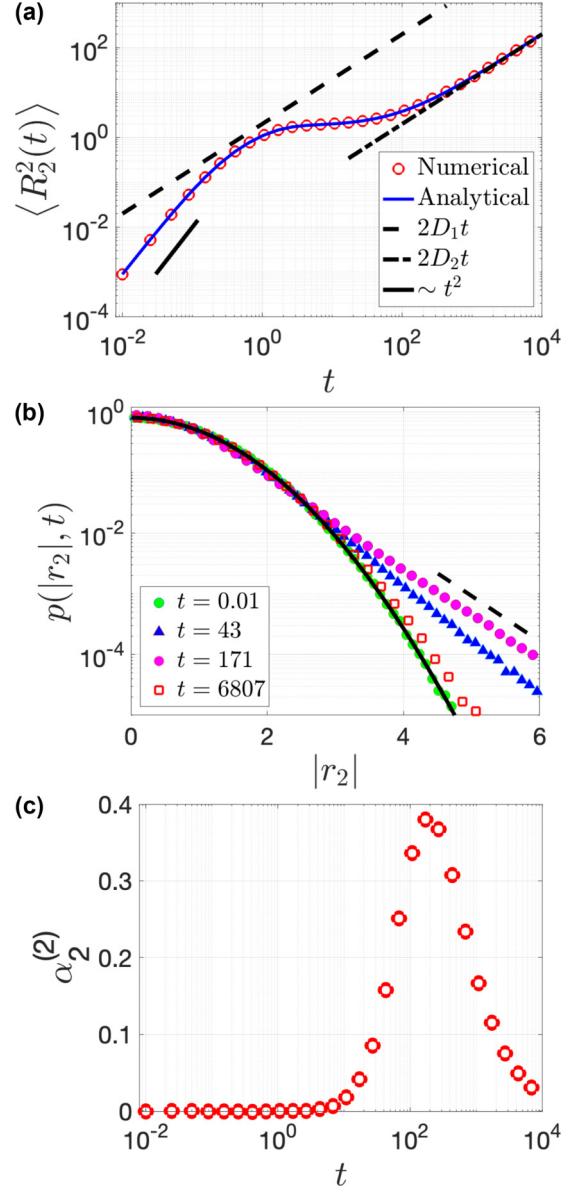


FIG. 3. FnGD transport properties for $n = 2$. Here, $dB_t^{(1)} = \sqrt{2D_1}dW_t^{(1)}$ and $dB_t^{(2)} = \sqrt{2D_2(t)}dW_t^{(2)}$, where $D_2(t) = D_2 y_t^2$ and y_t is an OU process with variance $\beta^2/2\lambda = 1$ (see text for details). (a) Analytical (solid blue line) and numerical (red circles) MSD profiles. Dashed and dashed-dotted lines indicate pure diffusion MSDs with $D_1 = 1$ and $D_2 = 0.01$, respectively, while the solid black line represents the ballistic MSD, i.e., $\text{MSD} \propto t^2$. (b) Scaled PDF vs scaled displacement. The solid black line is the standard normal, and the dashed black line represents an exponential tail. (c) NGP vs time. In all subfigures, the values of the parameters are $D_1 = 1$, $\gamma_1 = 10$, $D_2 = 0.01$, $\gamma_2 = 1$, $\lambda = 0.009$. Appendix A 4 provides details about the numerical methods and statistical average.

observed in disordered systems, especially in glass formers [20,24,26,50].

The transient deviation from Gaussian behavior is also captured by the nonmonotonic NGP shown in Fig. 3(c). Mathematically, this result can be easily understood. Initially, $\alpha_2^{(2)} = 0$ because the motion is predominantly governed by the pure BM $B_t^{(1)}$. However, after a relaxation period proportional

to γ_2^{-1} , the particle begins to follow the behavior of $B_t^{(2)}$, which displays a non-Gaussian behavior and as a result $\alpha_2^{(2)} \neq 0$. Over time, the NGP reaches a maximum and gradually returns to zero, indicating that the Gaussian behavior has been recovered. Similar to experimental and MD observations, the non-Gaussianity persists even after the particle enters the terminal diffusive regime. The position of the peak in $\alpha_2^{(2)}$ is controlled by the dissipation constant λ . Decreasing λ shifts the peak to longer times without affecting the MSD profile. By assuming that the noise terms $B_t^{(i)}$ in Eq. (1) have stochastic diffusivities, all the cases depicted in Fig. 1(c) and Fig. 2 can be endowed with the three characteristics of FnGD.

Interestingly, it is possible to generate a *strictly* Fickian diffusion (linear MSD profile) with transient non-Gaussian characteristics by implementing the same approach in Eq. (17) and setting $D_1 = D$ and $D_2(t) = Dy_t^2$. A similar result has also been obtained in a two-state model describing the diffusion of a particle in a field of dilute traps [44].

IV. SUMMARY AND DISCUSSION

This work proposes that particle motion in complex environments may be driven by a series of uncorrelated noise sources. This approach is physically motivated by an extension of kinetic theory and mathematically formulated as a series of hierarchically coupled random walks. By assuming that the noise sources are BM, the system can be expressed as a system of hierarchically coupled OU equations, which has an analytical solution for any number of noise sources. In the case of two noise sources, it was shown that this approach can describe three essential characteristics of FnGD: Fickian diffusion or transient subdiffusion, with non-Gaussian PDFs and nonmonotonic NGP. There have been many successful papers describing these aspects of FnGD using simple models based on CTRW, superstatistics, stochastic diffusivity, and their variations [16,30–44]. The present work is also characterized by its simplicity (a system of OU equations) and analytical expressions for MSD and autocorrelation functions.

Several interesting extensions of this work are currently being pursued and will be detailed in forthcoming publications. First, the current model can be easily extended to any dimension and for any n . It will be interesting to explore whether nonlinear coupling between different dimensions introduces additional complexity to the system [50] or if certain aspects of FnGD remain independent of dimensionality [26]. Second, different stochastic diffusivity approaches incorporating the CIR model [41] or mixtures of OU processes [16] accompanied by nonlinear force fields [51] may be used to finely tune the non-Gaussian characteristics of the motion. Third, the velocity ACF described by Eq. (15) also demonstrates intriguing characteristics. However, regardless of the parameter values, the long-term behavior of the ACF remains exponential, which does not capture the power-law relaxation observed in certain MD simulations. A potential solution to this problem would be to introduce memory effects in the form of power-law correlations in the drift terms of Eq. (1) [52]. This approach results in a system of hierarchically coupled generalized Langevin equations.

ACKNOWLEDGMENTS

The work was funded by National Science Foundation under Grant No. 1951583.

APPENDIX

1. Analytical solution for $n = 2$

The matrix $\mathbf{\Gamma}$ in Eq. (7) is diagonalizable with $\mathbf{\Gamma} = \mathbf{PAP}^{-1}$, where

$$\mathbf{A} = \begin{pmatrix} \gamma_1 & 0 \\ 0 & \gamma_2 \end{pmatrix}, \quad \mathbf{P} = \begin{pmatrix} \frac{1}{\bar{\gamma}} & 0 \\ 1 & 1 \end{pmatrix}, \quad \mathbf{P}^{-1} = \begin{pmatrix} \bar{\gamma} & 0 \\ -\bar{\gamma} & 1 \end{pmatrix},$$

and $\bar{\gamma} = \frac{\gamma_1}{\gamma_1 - \gamma_2}$. If $\gamma_1 = \gamma_2$, the system can still be solved analytically. This particular case will be discussed elsewhere. The matrix exponential is computed as $e^{\mathbf{\Gamma}t} = \mathbf{P}e^{\mathbf{A}t}\mathbf{P}^{-1}$, which yields the following result:

$$\mathbf{G}(t) = \begin{pmatrix} e^{-\gamma_1 t} & 0 \\ \bar{\gamma}(e^{-\gamma_1 t} - e^{-\gamma_2 t}) & e^{-\gamma_2 t} \end{pmatrix}. \quad (\text{A1})$$

Hence, Eq. (8) gives

$$u_t^{(1)} = u_0^{(1)}e^{-\gamma_1 t} + \sigma_1 \int_0^t e^{-\gamma_1(t-s)} dW_s^{(1)}, \quad (\text{A2})$$

and

$$\begin{aligned} u_t^{(2)} &= u_0^{(2)}e^{-\gamma_2 t} + \bar{\gamma}u_0^{(1)}(e^{-\gamma_1 t} - e^{-\gamma_2 t}) \\ &\quad + \bar{\gamma}\sigma_1 \int_0^t (e^{-\gamma_1(t-s)} - e^{-\gamma_2(t-s)}) dW_s^{(1)} \\ &\quad + \sigma_2 \int_0^t e^{-\gamma_2(t-s)} dW_s^{(2)}. \end{aligned} \quad (\text{A3})$$

The solutions for $X_t^{(i)}$ and $V_t^{(i)}$ with $i = 1, 2$ are derived from Eqs. (2) and (3), respectively.

By utilizing Eqs. (A3) and (2), we can derive the particle's displacement from the initial condition, $R_2(t) = X_t^{(2)} - X_0^{(2)}$:

$$\begin{aligned} R_2(t) &= u_0^{(2)}(1 - e^{-\gamma_2 t}) \\ &\quad + \sigma_2 \int_0^t (1 - e^{-\gamma_2(t-s)}) dW_s^{(2)} \\ &\quad + \bar{\gamma}u_0^{(1)}(e^{-\gamma_2 t} - e^{-\gamma_1 t}) \\ &\quad + \bar{\gamma}\sigma_1 \int_0^t (e^{-\gamma_2(t-s)} - e^{-\gamma_1(t-s)}) dW_s^{(1)}. \end{aligned} \quad (\text{A4})$$

2. Limit of large γ_1

In the limit of very large γ_1 , the first equation of Eq. (6) becomes $\gamma_1 u_t^{(1)} dt \approx \sigma_1 dW_t^{(1)}$. Thus the second equation of Eq. (4) reduces to

$$du_t^{(2)} = -\gamma_2 u_t^{(2)} dt - \sigma_1 dW_t^{(1)} + \sigma_2 dW_t^{(2)}, \quad (\text{A5})$$

and Eq. (1) becomes

$$dX_t^{(2)} = \gamma_2(B_t^{(2)} - X_t^{(2)})dt + dB_t^{(1)}, \quad (\text{A6})$$

Both Eqs (A5) and (A6) can be solved analytically:

$$u_t^{(2)} = u_0^{(2)} e^{-\gamma_2 t} - \sigma_1 \int_0^t e^{-\gamma_2(t-s)} dW_s^{(1)} + \sigma_2 \int_0^t e^{-\gamma_2(t-s)} dW_s^{(2)}, \quad (\text{A7})$$

and

$$R_2(t) = u_0^{(2)}(1 - e^{-\gamma_2 t}) + \sigma_1 \int_0^t e^{-\gamma_2(t-s)} dW_s^{(1)} + \sigma_2 \int_0^t (1 - e^{-\gamma_2(t-s)}) dW_s^{(2)}. \quad (\text{A8})$$

Note that due to the presence of a pure Brownian motion in Eq. (A6), the velocity of the particle, $V_t^{(2)}$, is not defined.

The equilibrium mean and variance of $u_t^{(2)}$ are $\mu = 0$ and $\beta = (\sigma_1^2 + \sigma_2^2)/2\gamma_2$, respectively. By applying Itô's integral properties and assuming that $\langle (u_0^{(2)})^2 \rangle = \beta$, the MSD presented in Eq. (18) can be derived.

3. Stochastic diffusivity

Let us assume that the diffusivity D_2 is modeled as a stochastic process given by $D_2(t) = D_2 y_t^2$, where y_t is an OU process with a variance of $\langle \delta y_t^2 \rangle_{\text{eq}} = \beta^2/2\lambda = 1$ (see Sec. III E for details). In other words, we have $\sigma_2(t) = \sigma_2 \sqrt{y_t^2}$. Under these assumptions, $\langle D_2(t) \rangle_{\text{eq}} = D_2$ and $\langle \sigma_2^2(t) \rangle_{\text{eq}} = \sigma_2^2$.

The only change required in the above derivations is that the stochastic integral

$$I_t = \sigma_2 \int_0^t e^{-\gamma_2(t-s)} dW_s^{(2)} \quad (\text{A9})$$

becomes

$$\tilde{I}_t = \int_0^t \sigma_2(s) e^{-\gamma_2(t-s)} dW_s^{(2)}. \quad (\text{A10})$$

While I_t is a Gaussian process, it is important to note that \tilde{I}_t does not exhibit Gaussian characteristics. Nevertheless, for a single stochastic path of y_t , the zero-mean and isometry properties of Itô integrals enable us to calculate the path-

conditional mean and variance:

$$\langle \tilde{I}_t | y \rangle = 0 \quad (\text{A11})$$

and

$$\langle \delta \tilde{I}_t^2 | y \rangle = \int_0^t \sigma_2^2(s) e^{-2\gamma_2(t-s)} ds, \quad (\text{A12})$$

respectively. Here, it is assumed that $W_t^{(2)}$ and y_t are independent. Consequently, by averaging over all stochastic paths of y_t , we obtain that

$$\langle \tilde{I}_t \rangle = 0, \quad (\text{A13})$$

and

$$\langle \delta \tilde{I}_t^2 \rangle = \sigma_2^2 \int_0^t e^{-2\gamma_2(t-s)} ds, \quad (\text{A14})$$

Therefore, even though the distributions of the observables are no longer Gaussian processes, the relationships for the MSD and velocity ACF remain unchanged.

4. Methods

The standard Euler-Maruyama method with a time step of $dt = 0.001$ was employed to solve all SDEs. In Fig. 2, the initial conditions for $u_t^{(i)}$ were sampled from a bivariate Gaussian distribution with zero mean and covariance given by Eq. (13). Without loss of generality, the following initial conditions were used: $X_0^{(i)} = 0$ and $B_0^{(i)} = u_0^{(i)}$. In the case of diffusing diffusivity (Fig. 3), the steady-state distribution deviates from a Gaussian. However, the initial conditions were sampled similarly to Fig. 2, but the system was allowed to equilibrate for 10^6 time-steps before commencing the sampling process.

The PDF of the particle's displacement was constructed by implementing the van Hove function,

$$P(R_2, t) = \frac{1}{M} \sum_{j=1}^M \langle \delta(R_2 - R_{2,j}(t)) \rangle, \quad (\text{A15})$$

where δ represents the delta function and M is the number of sampled points at time t .

- [1] R. Brown, *The Miscellaneous Botanical Works of Robert Brown: Vol. I* (The Ray Society, London, UK, 1866).
- [2] A. Einstein, On the motion of small particles suspended in a stationary liquid, *Ann. Phys.* **322**, 549 (1905).
- [3] M. von Smoluchowski, Zur kinetischen theorie der brownischen molekularbewegung und der suspensionen, *Ann. Phys.* **326**, 756 (1906).
- [4] P. Langevin, Sur la théorie du mouvement Brownien, *C. R. Acad. Sci. (Paris)* **146**, 530 (1908).
- [5] G. E. Uhlenbeck and L. S. Ornstein, On the theory of the Brownian motion, *Phys. Rev.* **36**, 823 (1930).
- [6] B. Wang, S. M. Anthony, C. B. Sung, and S. Granick, Anomalous yet Brownian, *Proc. Natl. Acad. Sci. USA* **106**, 15160 (2009).

- [7] B. Wang, J. Kuo, S. C. Bae, and S. Granick, When Brownian diffusion is not Gaussian, *Nat. Mater.* **11**, 481 (2012).
- [8] J. Hwang, J. Kim, and B. J. Sung, Dynamics of highly poly-disperse colloidal suspensions as a model system for bacterial cytoplasm, *Phys. Rev. E* **94**, 022614 (2016).
- [9] C. Di Rienzo, V. Piazza, E. Gratton, F. Beltram, and F. Cardarelli, Probing short-range protein Brownian motion in the cytoplasm of living cells, *Nat. Commun.* **5**, 5891 (2014).
- [10] M. E. Grady, E. Parrish, M. A. Caporizzo, S. C. Seeger, R. J. Composto, and D. M. Eckmann, Intracellular nanoparticle dynamics affected by cytoskeletal integrity, *Soft Matter* **13**, 1873 (2017).

- [11] J. Guan, B. Wang, and S. Granick, Even hard-sphere colloidal suspensions display Fickian yet non-Gaussian diffusion, *ACS Nano* **8**, 3331 (2014).
- [12] J. D. Eaves and D. R. Reichman, Spatial dimension and the dynamics of supercooled liquids, *Proc. Natl. Acad. Sci. USA* **106**, 15171 (2009).
- [13] S. Sengupta and S. Karmakar, Distribution of diffusion constants and Stokes-Einstein violation in supercooled liquids, *J. Chem. Phys.* **140**, 224505 (2014).
- [14] F. Sciortino, P. Gallo, P. Tartaglia, and S. H. Chen, Supercooled water and the kinetic glass transition, *Phys. Rev. E* **54**, 6331 (1996).
- [15] S. D. Overduin and G. N. Patey, An analysis of fluctuations in supercooled TIP₄P/2005 water, *J. Chem. Phys.* **138**, 184502 (2013).
- [16] S. Song, S. J. Park, M. Kim, J. S. Kim, B. J. Sung, S. Lee, J.-H. Kim, and J. Sung, Transport dynamics of complex fluids, *Proc. Natl. Acad. Sci. USA* **116**, 12733 (2019).
- [17] Z. Hu and C. J. Margulis, Heterogeneity in a room-temperature ionic liquid: Persistent local environments and the red-edge effect, *Proc. Natl. Acad. Sci. USA* **103**, 831 (2006).
- [18] L. Berthier and G. Biroli, Theoretical perspective on the glass transition and amorphous materials, *Rev. Mod. Phys.* **83**, 587 (2011).
- [19] L. Berthier and W. Kob, The Monte Carlo dynamics of a binary Lennard-Jones glass-forming mixture, *J. Phys.: Condens. Matter* **19**, 205130 (2007).
- [20] P. Chaudhuri, L. Berthier, and W. Kob, Universal nature of particle displacements close to glass and jamming transitions, *Phys. Rev. Lett.* **99**, 060604 (2007).
- [21] P. Charbonneau, Y. Jin, G. Parisi, and F. Zamponi, Hopping and the Stokes-Einstein relation breakdown in simple glass formers, *Proc. Natl. Acad. Sci. USA* **111**, 15025 (2014).
- [22] A. V. Orpe and A. Kudrolli, Velocity correlations in dense granular flows observed with internal imaging, *Phys. Rev. Lett.* **98**, 238001 (2007).
- [23] E. R. Weeks, J. C. Crocker, A. C. Levitt, A. Schofield, and D. A. Weitz, Three-dimensional direct imaging of structural relaxation near the colloidal glass transition, *Science* **287**, 627 (2000).
- [24] F. Rusciano, R. Pastore, and F. Greco, Fickian Non-Gaussian diffusion in glass-forming liquids, *Phys. Rev. Lett.* **128**, 168001 (2022).
- [25] W. K. Kegel, Direct observation of dynamical heterogeneities in colloidal hard-sphere suspensions, *Science* **287**, 290 (2000).
- [26] F. Rusciano, R. Pastore, and F. Greco, Universal evolution of Fickian non-Gaussian diffusion in two- and three-dimensional glass-forming liquids, *Int. J. Mol. Sci.* **24**, 7871 (2023).
- [27] C. Xue, X. Zheng, K. Chen, Y. Tian, and G. Hu, Probing non-Gaussianity in confined diffusion of nanoparticles, *J. Phys. Chem. Lett.* **7**, 514 (2016).
- [28] A. Alexandre, M. Lavaud, N. Fares, E. Millan, Y. Louyer, T. Salez, Y. Amarouchene, T. Guérin, and D. S. Dean, Non-Gaussian diffusion near surfaces, *Phys. Rev. Lett.* **130**, 077101 (2023).
- [29] R. Pastore, A. Ciarlo, G. Pesce, F. Greco, and A. Sasso, Rapid Fickian yet non-Gaussian diffusion after subdiffusion, *Phys. Rev. Lett.* **126**, 158003 (2021).
- [30] E. W. Montroll and G. H. Weiss, Random walks on lattices. II, *J. Math. Phys.* **6**, 167 (1965).
- [31] P. Chaudhuri, Y. Gao, L. Berthier, M. Kilfoil, and W. Kob, A random walk description of the heterogeneous glassy dynamics of attracting colloids, *J. Phys.: Condens. Matter* **20**, 244126 (2008).
- [32] M. Hidalgo-Soria, E. Barkai, and S. Burov, Cusp of non-Gaussian density of particles for a diffusing diffusivity model, *Entropy* **23**, 231 (2021).
- [33] O. Rubner and A. Heuer, From elementary steps to structural relaxation: A continuous-time random-walk analysis of a supercooled liquid, *Phys. Rev. E* **78**, 011504 (2008).
- [34] J. Helfferich, F. Ziebert, S. Frey, H. Meyer, J. Farago, A. Blumen, and J. Baschnagel, Continuous-time random-walk approach to supercooled liquids. II. Mean-square displacements in polymer melts, *Phys. Rev. E* **89**, 042604 (2014).
- [35] E. Barkai, R. Metzler, and J. Klafter, From continuous time random walks to the fractional Fokker-Planck equation, *Phys. Rev. E* **61**, 132 (2000).
- [36] E. Barkai, CTRW pathways to the fractional diffusion equation, *Chem. Phys.* **284**, 13 (2002).
- [37] B. B. Mandelbrot and J. W. V. Ness, Fractional Brownian motions, fractional noises, and applications, *SIAM Rev.* **10**, 422 (1968).
- [38] R. Metzler, J. H. Jeon, A. G. Cherstvy, and E. Barkai, Anomalous diffusion models and their properties: Non-stationarity, non-ergodicity, and ageing at the centenary of single particle tracking, *Phys. Chem. Chem. Phys.* **16**, 24128 (2014).
- [39] C. Beck and E. G. Cohen, Superstatistics, *Physica A* **322**, 267 (2003).
- [40] R. Metzler, Superstatistics and non-Gaussian diffusion, *Eur. Phys. J.: Spec. Top.* **229**, 711 (2020).
- [41] M. V. Chubynsky and G. W. Slater, Diffusing diffusivity: A model for anomalous, yet Brownian, diffusion, *Phys. Rev. Lett.* **113**, 098302 (2014).
- [42] A. V. Chechkin, F. Seno, R. Metzler, and I. M. Sokolov, Brownian yet non-Gaussian diffusion: From superstatistics to subordination of diffusing diffusivities, *Phys. Rev. X* **7**, 021002 (2017).
- [43] Y. Lanoiselée and D. S. Grebenkov, A model of non-Gaussian diffusion in heterogeneous media, *J. Phys. A: Math. Theor.* **51**, 145602 (2018).
- [44] S. Mora and Y. Pomeau, Brownian diffusion in a dilute field of traps is Fickian but non-Gaussian, *Phys. Rev. E* **98**, 040101(R) (2018).
- [45] L. C. Evans, *An Introduction to Stochastic Differential Equations* (American Mathematical Society, Providence, RI, 2013).
- [46] A Brownian motion path is nowhere differentiable, which implies sharp changes in direction (infinite velocity). Collisions with other fluid molecules represent the most sudden change in velocity. Realistically, this change is not infinite but is remarkably sharp. Thus, collision points may be considered as part of a Brownian motion path.
- [47] H. Qian, Mathematical formalism for isothermal linear irreversibility, *Proc. R. Soc. A* **457**, 1645 (2001).

- [48] C. Godrèche and J. M. Luck, Characterising the nonequilibrium stationary states of Ornstein-Uhlenbeck processes, *J. Phys. A: Math. Theor.* **52**, 035002 (2019).
- [49] G. Porpora, F. Rusciano, V. Guida, F. Greco, and R. Pastore, Understanding charged vesicle suspensions as Wigner glasses: Dynamical aspects, *J. Phys.: Condens. Matter* **33**, 104001 (2021).
- [50] J. M. Miotto, S. Pigolotti, A. V. Chechkin, and S. Roldán-Vargas, Length scales in Brownian yet non-Gaussian dynamics, *Phys. Rev. X* **11**, 031002 (2021).
- [51] K. Toman and N. K. Voulgarakis, Stochastic pursuit-evasion curves for foraging dynamics, *Physica A* **597**, 127324 (2022).
- [52] T. Sandev and Z. Tomovski, Langevin equation for a free particle driven by power law type of noises, *Phys. Lett. A* **378**, 1 (2014).

Correction: A typographical error in Sec. II heading has been fixed. The sum in Eq. (5) and the matrix in Eqs. (10) and (11) contained errors and have been fixed. In Sec. 1 of the Appendix, the matrix exponential in the fourth sentence of the Appendix has been fixed, and the subscript t has been fixed to subscript s in Eqs. (A4) and (A8).

Second Correction: The fix to Eq. (5) in the First Correction was implemented incorrectly and has now been set right.